Applied Surface Science 393 (2017) 127–133

Contents lists available at ScienceDirect

Applied Surface Science

journal homepage: www.elsevier.com/locate/apsusc

Full length article

Morphology control in thin films of PS:PLA homopolymer blends by dip-coating deposition

Alexane Vital[a,b], Marylène Vayer[a], Thomas Tillocher[b], Rémi Dussart[b], Mohamed Boufnichel[c], Christophe Sinturel[a,*]

[a] Interfaces, Confinement, Matériaux et Nanostructures (ICMN), CNRS-Université d'Orléans, UMR 7374, 1B Rue de la Férollerie, C.S. 40059, 45071 Orléans Cedex 2, France
[b] Groupe de recherches sur l'énergétique des milieux ionisés (GREMI), CNRS-Université d'Orléans, UMR 7344, 14 rue d'Issoudun, B.P. 6744, F45067 Orléans Cedex 2, France
[c] STMicroelectronics, 16, rue Pierre et Marie Curie, B.P. 7155, 37071 Tours Cedex 2, France

ARTICLE INFO

Article history:
Received 4 July 2016
Received in revised form 2 September 2016
Accepted 28 September 2016
Available online 30 September 2016

Keywords:
Polymer blend
Dip-coating
Morphology
Thin polymer film
Phase separation

ABSTRACT

In this work, smooth polymer films of PS, PLA and their blends, with thicknesses ranging from 20 nm up to 400 nm and very few defects on the surface were obtained by dip-coating. In contrast to the process of spin-coating which is conventionally used to prepare thin films of polymer blends, we showed that depending on the deposition parameters (withdrawal speed and geometry of the reservoir), various morphologies such as layered films and laterally phase-separated domains could be formed for a given blend/solvent pair, offering much more opportunities compared to the spin-coating process. This diversity of morphologies was explained by considering the superposition of different phenomena such as phase separation process, dewetting and vitrification in which parameters such as the drying time, the compatibility of the polymer/solvent pairs and the affinity of the polymer towards the interfaces were suspected to play a significant role. For that purpose, the process of dip-coating was examined within the capillary and the draining regimes (for low and high withdrawal speed respectively) in order to get a full description of the thickness variation and evaporation rate as a function of the deposition parameters.
© 2016 Published by Elsevier B.V.

1. Introduction

When a blend of immiscible homopolymers is deposited from a solution of the polymers in a common solvent, the morphology of the film after drying results from the superposition of complex phenomena such as phase separation process, dewetting and vitrification of the system. Depending on the evaporation rate, the phase separation and the dewetting can be stopped into more or less advanced stages [1–8]. This provides a wide variety of thin film morphologies including co-continuous or dis-continuous laterally phase-separated morphologies as well as layered systems. The compositional heterogeneities length scale can vary from few tens of nanometers to several microns [9]. When deposited by spin-coating, it is rather difficult to vary significantly the deposition parameters for a given polymer/solvent pair, and post-treatments are often necessary to direct the morphology in the film (like thermal or solvent – SVA – annealing) [10]. On the other hand, it is now well established that experimental conditions in dip-coating such as the withdrawal speed, the nature of the solvent, or the concentration of the solvent vapors above the reservoir can be tuned in order to significantly influence the properties of the final dried films [11–13]. Studying dip-coating from sol-gel solutions, Faustini et al. [11] demonstrated that within withdrawal speed from 0.01 to 20 mm s^{-1} deposition occurs in two specific regimes, namely the capillary and the draining regimes (for low and high withdrawal speed respectively). The physical processes of the film formation are different [14], leading to a "V" shaped thickness evolution. Extensively studied in the case of sol-gel process, the dip-coating of polymer solutions has been reported for a limited number of examples including photovoltaic applications [13,15] or block copolymer thin films [12,16–19]. Very recently, it has been demonstrated in a series of papers by Roland et al. [12,20,21] that the "V" shaped thickness evolution for supramolecular block copolymer films formed by dip-coating was verified. It was also shown in these works that the morphology was highly influenced by the withdrawal speed, allowing for morphology control in a very simple way, without the need of additional post-annealing techniques.

* Corresponding author.
E-mail address: christophe.sinturel@univ-orleans.fr (C. Sinturel).

http://dx.doi.org/10.1016/j.apsusc.2016.09.151
0169-4332/© 2016 Published by Elsevier B.V.

In this work, we have exploited the versatility of the deposition process by dip-coating in order to direct the morphology in thin films of polymer blends. We focused our investigation on blends of polystyrene (PS) and polylactic acid (PLA) that can be used, in case of a laterally phase separated morphology, as masks for etching as demonstrated in previous work from our group [22]. We varied the type of solvent used to prepare the polymer solution, the withdrawal speed and also the configuration of the reservoir containing the solution to be deposited in order to generate various evaporation conditions. Dip-coating of polymer blends using such a large variety of deposition speed and solvent quality has, to the best of our knowledge, not been yet reported. In the first part of the paper, we focus on the thickness variations of the film as a function of the deposition parameters. In the second part, we examine the morphology of two PS and PLA blends.

2. Experimental

2.1. Materials

Polystyrene (PS), polylactic acid (PLA) respectively with molar weight of 350 and 95 kg·mol^{-1} were used. All the used solvents were purchased from Sigma Aldrich and used as received. In a 6" wafer of Si(100) supplied by MEMC Electronic Materials, substrates of 10*60 mm^2 were prepared. Because it is known that the oxide layer nature at the top of the Si substrate can deeply influence the wetting behavior and therefore the morphology of heterogeneous polymer systems deposited as thin films [23], all samples were prepared from a same single wafer to ensure the reproducibility of the surface composition. All samples were cleaned using the exact same procedure by sonication in dichloromethane, methanol, distilled water for 10 min each, dried under dry nitrogen gas for one minute and used straight away. The contact angle with water after this preparation was 71 ± 2° on all prepared samples.

2.2. Polymers thin film solution

Solutions of PS and PLA were prepared by dissolving the adequate mass of polymer in solvent (toluene, 1,2-dichloroethane (DCE), or tetrahydrofuran (THF)) to obtain a concentration of polymer of 30 mg·mL^{-1}. The solutions were stirred at least 2 h. Solutions of PS and PLA blends were prepared in the same way: PS and PLA were weighted in order to get the adequate polymer concentration (30 mg·mL^{-1}) and mass ratio (namely PS:PLA 70:30 and 30:70) and dissolved in solvent (toluene, DCE, or THF). The solutions were stirred at least 2 h.

2.3. Dip-coating procedure

The films were prepared by dip-coating Si substrates using a homemade equipment. The container of the polymers solution was a graduated cylinder. The dimension of the graduated cylinder are: 7.5 cm high and 1.7 cm internal diameter. Two configurations of filling were used: completely or half filled (named "full" and "half" respectively). In both configurations, the Si substrate was immersed in the solution on 4 cm high. It was left immersed one minute. This time allows all perturbations due to the immersion of the substrate to be fully damped. Then, the substrate was pulled out at constant speed between 1 and 500 mm min^{-1}.

2.4. Thickness evaluation

The film thickness was evaluated using an interference-based film thickness measurement system (F20, Filmetrics) for the PS and PLA homopolymer films. For films of PS:PLA blends, the thickness cannot be evaluated with interference-based thickness measurement system. The thickness of these films was thus evaluated only using AFM profiles. A typical on dimensional line-cut in shown in Fig. S1 (SI).

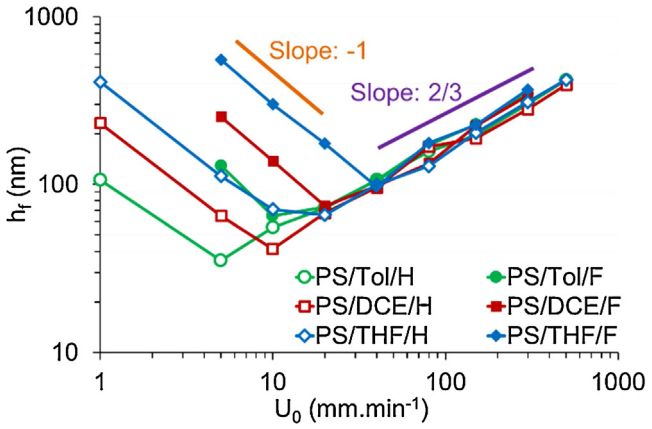

Fig. 1. Thickness (h_f) as a function of withdrawal speed (U_0) for PS solutions in toluene (circles), DCE (squares) and THF (diamonds) in "half" (H) (open marks) and "full" (F) configuration (full marks).

2.5. Atomic force microscopy images

Atomic Force Microscopy (AFM) images were collected using a Molecular Imaging Pico+ in contact mode. Only height images were recorded. For morphologies showing circular domains, AFM images were thresholded in order to get binary images and evaluate the characteristics of the discrete domains. The area, length and geometric centres of the discrete domains were determined using Image J software [1] and the domains were fitted by an ellipse. The size of the domains was calculated as the mean between the lengths of the major and the minor axes. The films were scratched after dip-coating in order to uncover partially the bare substrate. The scratched area was imaged by AFM and cross section profiles were performed. The corresponding profiles were used to evaluate the thicknesses of the films, which are in agreement with those evaluated with the interference-based thickness measurement system for PS and PLA films. An example of the process flow as well as typical histogram is provided in Fig. S2 (SI).

2.6. Selective elimination of one polymer

PLA and PS were eliminated by depositing respectively a drop of glacial acetic acid or tetrachloroethylene onto the film during 15 s and wiping it out through an N_2 flow.

2.7. Determination of the film drying time

To determine the film drying time, solution contained only one polymer (PS or PLA) is used. Videos of the withdrawing samples at 5 and 80 mm min^{-1} were recorded. The height position of the drying line on the withdrawing sample was visually located by a sharp colour change on the sample. The height difference between the solution and this line was measured. The drying time was calculated from this height difference and the withdrawal speed.

3. Results and discussion

Fig. 1 shows the typical variation of the polymer film thickness (after drying) as a function of the withdrawal speed. The results shown here were obtained with pure PS deposited by dip-coating from solutions in three solvents (Toluene, Tetrahydrofuran (THF)

Table 1
D_{fit} (10^{-4} $m^{1/3}\cdot s^{2/3}$), E_{fit} (10^{-12} $m^3\cdot s^{-1}$), E_5 (10^{-12} $m^3\cdot s^{-1}$) and E_{80} (10^{-12} $m^3\cdot s^{-1}$) for PS and PLA solutions in toluene, DCE, THF for the "full" and "half" configurations.

	FULL					HALF			
Polymers	Solvent	D_{fit}	E_{fit}	E_5	E_{80}	D_{fit}	E_{fit}	E_5	E_{80}
PS	Toluene	4.0 ± 0.5	3 ± 1	3 ± 1	12 ± 5	3.5 ± 0.5	0.6 ± 0.5	0.4 ± 0.1	4 ± 1
PS	DCE	3.8 ± 0.5	6 ± 1	7 ± 2	12 ± 6	3.2 ± 0.5	1.3 ± 0.5	1.1 ± 0.4	6 ± 2
PS	THF	4.1 ± 0.5	15 ± 1	25 ± 9	25 ± 15	3.4 ± 0.5	2.2 ± 0.5	3 ± 1	6 ± 2
PLA	Toluene	3.0 ±0.5	3 ± 1	2 ± 1	6 ± 2	3.1 ± 0.5	0.6 ± 0.5	0.2 ± 0.1	2.0 ± 0.7
PLA	DCE	3.5 ± 0.5	7 ± 1	5 ± 2	8 ± 4	3.0 ±0.5	1.4 ± 0.5	0.5 ± 0.2	2.2 ± 0.8
PLA	THF	3.5 ± 0.5	17 ± 1	14 ± 5	11 ± 5	2.7 ± 0.5	2.5 ± 0.5	1.9 ± 0.7	3 ± 1

and 1,2-dichloroethane (DCE)) using the "full" and "half" deposition configurations. As already shown in similar works using polymer solutions [12,20,21], the thickness versus withdrawal speed in a log/log scale exhibits a "V" shaped curve. It decreases with increasing speed at low speed, goes through a minimal thickness for a critical speed, and increases for higher values of the speed. The curves relative to the PLA, PS:PLA 70:30 and 30:70 blends are shown in SI (Figs. S3–S5) and exhibit the same kind of behavior.

For high withdrawal speed, the formation of the liquid film on the substrate results from the balance between the viscous drag of the solution and capillary forces which are opposed to the deformation of the meniscus. The geometry and dimension of the resulting meniscus which is of high importance in this process has been already described in details in the literature [14,24–26]. The moving substrate takes off the liquid from the surface of the bath until a critical point (generally named stagnation point) where the solution goes back into the bath due to the domination of the gravity forces [14]. In this so-called draining regime, the thickness (h_0) of the liquid film withdrawn from the reservoir can be described by the Landau-Levich Eq. (1) [14,24–26] considering a Newtonian and non-evaporating liquid:

$$h_0 = 0.94\frac{(\eta_s U_0)^{2/3}}{\gamma_s^{1/6}(\rho_s g)^{1/2}} \quad (1)$$

with η_s, γ_s and ρ_s being the viscosity, the surface tension and the density of the liquid, U_0 and g being the withdrawal speed and standard gravity respectively.

In our case, the solvent is evaporating and the non-volatile species are progressively concentrated until the point where a dried film with a thickness h_f is formed. In these conditions, the thickness of the film h_f can no longer be expressed with Eq. (1) but has still a 2/3 power-law dependence on the withdrawal speed [11,27,28]. The final thickness can be expressed by Eq. (2) that takes into account the evaporation of the solvent as proposed by Faustini et al. [11]

$$h_f = k_i D U_0^{2/3} \quad (2)$$

where k_i represents the volume proportion of the non-volatile compounds in the solution, D is a global draining constant. k_i can be calculated in our case by $k_i = c_i/\rho_i$ where c_i and ρ_i being the mass concentration of the polymer in the solution ($g\,cm^{-3}$) and the density of the polymer ($g\cdot cm^{-3}$) respectively.

At low withdrawal speed, the evaporation phenomenon is dominant and induces a capillary flow that drags the solution from the bath towards the upper part of the meniscus. This leads to an accumulation of the non-volatile species which in turn favors the formation of higher thicknesses. This trend can be described by Eq. (3) [11,27].

$$h_f = k_i \frac{E}{L}\frac{1}{U_0} \quad (3)$$

with E, L being the evaporation rate and the film width, respectively. In this model, the dried film thickness is proportional to the inverse of the withdrawal speed.

For very low withdrawal speed ($1\,mm\,min^{-1}$), stripes are formed at the surface of the film, perpendicularly to the withdrawal direction (Fig. S6a). This phenomenon, called "stick-slip motion" has been observed and described by Huang et al., Ghosh et al. and Uchiyama et al. [29–31] and occurs when high concentrations of non-volatile compounds are formed and pinned in the upper part of the meniscus, leading to the formation of local thickness heterogeneities (Fig. S6b).

Combining the two models of Eqs. (1) and (3) permits to describe the variation of the film thickness over the whole range of withdrawal speed (Eq. (4)) [11].

$$h_f = k_i\left(\frac{E}{L}\frac{1}{U_0} + D U_0^{2/3}\right) \quad (4)$$

In our case, we have verified that the thickness variation with the withdrawal speed exhibits a slope close to 2/3 and -1 in the draining and capillary regime respectively (see Fig. 1). The curves of the thickness versus withdrawal speed relative to PS and PLA films were fitted using Eq. (4). From the fits, we were able to extract the values of the draining constant D_{fit} and evaporation rate E_{fit} for each polymer/solvent pair, in the two types of deposition configuration "full" and "half" (Table 1).

The draining constant D_{fit} was found to be slightly affected by the type of solvent for a given polymer but was found to be lower for PLA compared to PS. This could be related to the lower molecular mass of PLA inducing a lower viscosity of the solution. In contrast, it can be observed that the configuration and the nature of the solvent strongly affected the evaporation rate E_{fit}. Three main parameters were found to play a central role:

1. *The deposition configuration*: the evaporation rates are lower in the "half" configuration compared to the "full" one for a given polymer/solvent pair. This is consistent with the presence of higher vapor pressure inside the cylinder due the confinement of the atmosphere which induces a reduced evaporation rate.
2. *The vapor pressure of the solvent*: for a given polymer, the evaporation rate increases with higher vapor pressure (P^0_{THF} (193 hPa) > P^0_{DCE} (87 hPa) > $P^0_{Toluene}$ (29 hPa) at 20 °C induces $E_{THF} > E_{DCE} > E_{toluene}$).
3. *The affinity of the solvent towards the polymer*: which is known to affect the rate of the solvent removal in the general case of the polymer film formation [32]. We estimated for that purpose the swelling ratio of a polymer film exposed to solvent vapor at a given partial pressure, that gives a measure of the polymer/solvent affinity. The swelling ratio for PS and PLA films evaluated in such way at $p/p^0 = 0.95$, are respectively 1.8, 1.9 for toluene, 2.5, 3.0 for THF and 2.0, 3.0 for DCE. Consideration of these values shows that toluene, THF and DCE are more selective to PLA than PS. This explains why the evaporation rates are lower with PLA.

The fitted values of the evaporation rate were compared to experimental values determined from videos of the substrate withdrawing from the solution. From the height position of the drying

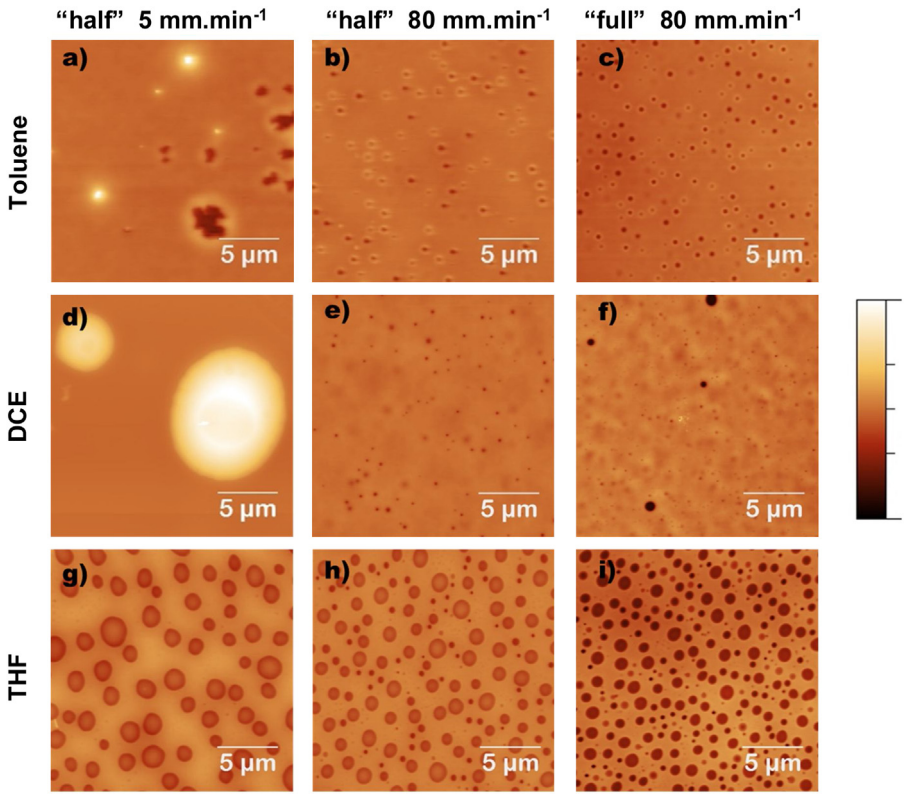

Fig. 2. 20 × 20 µm AFM images of PS:PLA(70:30) blend films (a), (b), (c) in toluene; (d), (e), (f) in DCE; (g), (h), (i) in THF; (a), (d), (g) at a 5 mm·min^{-1} in configuration "half"; (b), (e), (h) at 80 mm·min^{-1} in configuration "half"; c), (f), (i) at 80 mm·min^{-1} in configuration "full". The Z scale is −50 to +50 nm for all images except for image d) (−500 to +500 nm).

line on the withdrawing sample (visually located by a sharp color change of the substrate on the video), the drying time (t_D) was extracted on the video by time monitoring. During this drying time, the amount of solvent to be evaporated could be estimated considering that the solution to be dried is located between the solution and the maximal height of the meniscus (approximated to the capillary length l_C).[33] Consequently, the evaporation rate could be estimated using Eq. (5).

$$E = \frac{(h_s - h_f) l_C L}{2 t_D} \tag{5}$$

with h_s thickness at the base of the solution, L width of the sample.

Two withdrawal speeds were investigated: 5 mm·min^{-1} within the capillary regime and 80 mm·min^{-1} within the draining regime leading to the determination of E_5 and E_{80} respectively. The results displayed in Table 1 show a good agreement between E_{fit} and E_5, those two values being considered in the capillary domains (low withdrawal speed). In contrast, E_{80} differs from E_{fit} (or E_5) which indicates that the evaporation rate (E) depends on the withdrawal speed in our experimental conditions. In the two configurations $E_{80} > E_5$ suggesting that the vapor pressure above the reservoir is not homogenous: at high speed, the sample dries far away from the surface where the concentration of solvent vapor is low whereas at low speed, the sample dries close to the reservoir surface where the concentration of solvent vapor is higher. This effect is minimized in the "full" configuration where the vapor pressure gradient is expected to be sharper (vapor pressure is already low for E_5). The difference between E_{80} and E_5 depends also on the intrinsic evaporation of the solvent (vapor pressure) and is reduced for solvent with high evaporation rate such as THF. The evaporation rates are lower for PLA than for PS indicating a better solvent retention in PLA than in PS film. Although we show that E depends on U, Eq. (4) is still valid with E being taken in the capillary regime since the first tem of Eq. (4) vanished at higher speed values.

Finally, we have examined the position of the critical speed (U_c) which corresponds to the withdrawal speed at the point where both regimes compensate and the thickness reaches a minimum value (minimum of the curves in Fig. 1). From the derivative of the Eq. (4) (Eq. (6)), it can be seen that U_c is only a function of the evaporation rate of the solvent (E), L and D being both constant in our experimental conditions:

$$U_c = \left(\frac{2}{3}\frac{E}{L\ D}\right)^{3/5} \tag{6}$$

As seen in Table 1, the evaporation rate increases in the order Tol < DCE < THF. Consequently, the characteristic speed increases in the same order as seen in Fig. 1 where the minimum of the curves is shifted to the right part of the diagram in the order Tol, DCE, THF.

We now present and discuss the different types of morphologies observed by AFM in thin films composed of blends of PS and PLA deposited from solutions in the various organic solvents. Figs. 2 and 3 illustrate the different types of morphology that can be obtained by changing the parameters of deposition (withdrawal speed and configuration of the reservoir) and the characteristics of the solution (type of solvent, composition of the blends). The two first columns correspond to the configuration "half", in the capillary regime (5 mm·min^{-1}) and in the draining regime (80 mm·min^{-1}). The third column corresponds to the configuration "full", only showing the morphology obtained in the draining regime (80 mm·min^{-1}) since the morphology was found to be independent with the regime of deposition (see Figs. S7 and S8 in the SI). The three lines correspond to the three different solvents used for the preparation of the solution (toluene, DCE, THF). From the selective extraction of PLA (using acetic acid) and PS (using tetrachloroethylene) coupled with the AFM observations of the resulting

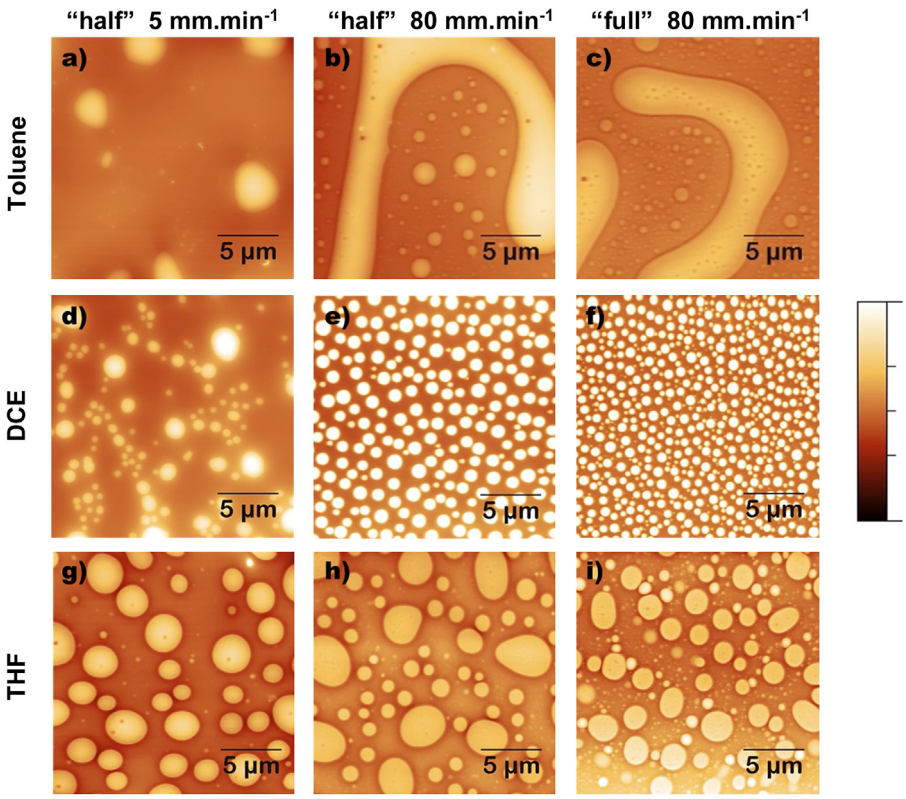

Fig. 3. 20 × 20 µm AFM images of PS:PLA(30:70) blend films (a), (b), (c) in toluene; (d), (e), (f) in DCE; (g), (h), (i) in THF; (a), (d), (g) at a 5 mm·min^{-1} in configuration "half"; (b), (e), (h) at 80 mm·min^{-1} in configuration "half"; c), (f), (i) at 80 mm min^{-1} in configuration "full". The Z scale is −50 to +50 nm for all images except for image a) and d) (−150 to +150 nm).

morphologies, we were able to determine the repartition of the polymer in the film for each situation.

Fig. 2 shows representative images of the surface morphology obtained by AFM for PS:PLA (70:30) blend. For the films obtained from toluene solution, the featureless morphology of Fig. 2a was attributed to the formation of stratified domains with layers (from the top to the bottom) of PS and PLA as revealed by a global thickness decrease after two successive extractions with tetrachloroethylene and acetic acid. Similar behaviors were observed with samples shown in Fig. 2b and c, although the stratification was less perfect as judged by the presence of discontinuations in the upper PS layer which can be attributed to specific interactions between the polymer phases during the process of the layers formation.

For the films obtained from DCE solution, a stratified morphology was also found in the case of the morphologies depicted in Fig. 2e and f, but in this case, the identification of the polymer location revealed the presence (from the top to the bottom) of a first thin layer of PLA, followed by PS layer and then PLA layer again as a wetting layer on the substrate surface. In this case, we now describe the process flow for the qualitative and quantitative characterization of the different layers based on the successive elimination using selective solvent. Fig. S9 in SI shows the evolution of the cross section profile of the films during this process. It can be seen in this example that the film thickness decreases from 170 nm to 165 nm after a first selective extraction with acetic acid (selective to PLA). A second extraction with tetrachloroethylene (selective to PS) leads to a film thickness of 45 nm. A third extraction with acetic acid (selective to PLA) removes the remaining layer. This leads to the conclusion that the initial film with a thickness of 170 nm is composed of a 5 nm layer of PLA on top of a 120 nm layer of PS and 45 nm PLA bottom wetting layer. For a more accurate, direct and non-destructive vertical assessment of compositional heterogeneities, it has to be noted that grazing incidence techniques such as X-ray reflectivity and GISAXS are ideal tools. We refer the interested readers to the following literature that describes selected examples of such approach [34,35]. Finally, the morphology observed in Fig. 2d was attributed to large PS islands surrounding by a matrix of PLA.

For the films obtained from THF solution, the presence of discrete PLA domains dispersed in a continuous matrix of PS was revealed (Fig. 2g–i). The selective extraction of the PLA led to cylindrical cavities, which depth matches the thickness of the film, indicating that the PLA went through the entire PS phase. It was found that the dimensions of the PLA domains were influenced by the parameters of the deposition. The mean diameters of the PLA domains in Fig. 2g–i were respectively 1.6 µm, 740 and 650 nm. Interestingly, these results are in line with earlier work from the Muller-Buschbaum group showing the strong dependence between morphology and i) layer thickness [36] on one hand and ii) shape of the meniscus on the other hand [37] which are two parameters that are clearly affected by the deposition conditions in dip-coating. This confirms that the use of dip-coating, allowing for preparation of thin films in various conditions by changing the withdrawal speed is of high importance to simply control the morphology of the deposited film.

Fig. 3 shows representative images of the surface morphology obtained by AFM for a PS:PLA (30:70) blend obtained in the conditions already described for Fig. 2. Again, we were able to assign the polymer phases on the basis of the AFM observation of the film after successive selective extractions. For all the configurations, no stratified morphology was observed using this blend composition. Discontinuous PS domains dispersed within a continuous matrix of

PLA were observed, with shape and dimensions depending on the deposition parameters.

For the films obtained from toluene solution, more or less elongated discontinuous PS domains were formed for all conditions (Fig. 3a–c). The selective removal of the phases revealed a wetting layer of PLA on the Si substrate indicating that the PS domains were not going through the entire PLA phase.

For the films obtained from DCE solution, cylindrical domains of PS were observed with a mean diameter of 0.9 and 1.6 μm (bimodal distribution), 800 and 650 nm in Fig. 3d–f respectively. Similar to toluene, a wetting layer of PLA on the Si substrate was identified by the successive selective extractions but in this case, an additional thin PLA layer covering the discontinuous PS domains was observed.

For the films obtained from THF solution, cylindrical domains were observed with a mean diameter of 1.9, 1.0 and 2.5 (bimodal distribution), 1.2 μm in Fig. 3g–i respectively but in this case it was found that the PS domains were going through the entire PLA phase, with no formation of a continuous PLA wetting layer.

Since the films were deposited from homogeneous solutions of the polymers in a common solvent, the final dried morphology resulted from the competition between phase separation of the polymers (induced by the evaporation) and the vitrification of the system. It can be thus anticipated that the relative position of the onset of the phase separation and the vitrification will determine the extent of the phase separation and will drive parameters such as the shape and the dimension of the domains in the dried state. Additionally, specific interactions from the polymers toward the interfaces (free surface and film/substrate interface) will favor the formation of stratified morphology versus laterally phase separated domains [9]. We consequently expect that the morphology observed in Figs. 2 and 3 can be explained in terms of the drying time, the compatibility of the solvent/polymer pairs and the affinity of the polymer towards the interfaces. In the following, we discuss these parameters for each of the three solvents used in this study.

A laterally phase separated morphology with discrete domains is observed with THF. As judged by the values of the Flory-Huggins parameters (χPS/THF = 0.05, χPLA/THF = 0.01), THF can be considered as a good solvent for both PS and PLA, that produces PS-rich and PLA-rich phases equally swollen after phase separation. This mediates the surface energy of the swollen system, favoring a mixed distribution of polymer phases at both interfaces (silicon/polymer and surface of the film). Additionally, the high solubility of both polymers in THF delays the phase separation towards more concentrated solution, meaning high evaporation level, potentially very close to the vitrification point of the system. The combination of these two phenomena favors the formation of laterally phase separated domains going through the entire film thickness (Figs. 2g–i, 3g–i). For a given deposition condition, the behaviors of the PS:PLA (70:30) and (30:70) blends are similar (laterally phase separated morphology) but not fully symmetric due to the mobility difference of the PLA versus PS chains and asymmetry of the phase diagram. Very interestingly, it can be noted that for a given composition of the solution, different morphological characteristics can be obtained (here the domain size) by changing the deposition parameters. Higher evaporation rate favors the formation of domains with smaller dimensions, due to the limitation of the phase separation progress. Such variety of morphology for the same solution cannot be achieved and well controlled using spin coating.

In contrast, toluene can be considered as a poorer solvent than THF for both PS and PLA ($\chi_{PS/Toluene}$ = 0.5, $\chi_{PLA/Toluene}$ = 0.5). The limited solubility of both polymers in toluene favors the phase separation for low evaporation level, allowing for diffusion and coalescence phenomena of separated phases. During the phase separation, a PLA wetting layer on the silicon is formed, driven by the small surface energy between PLA (39 mN m^{-1}) and Si (36 mN m^{-1}) inducing the formation of a PS-rich surface layer in contact with the solvent in the same time. Layered morphology (PS layer on the top of PLA layer) is obtained for a composition where PS is the major component (PS:PLA (70: 30)) (Fig. 2a–c). When PLA is the major component, PS forms discrete domains resulting from the dewetting of the PS layer above the PLA layer (Fig. 3a–c).

DCE provides a third type of behavior where the two polymers display a different affinity towards the solvent. DCE is a good solvent for PLA ($\chi_{PLA/DCE}$ = 0.01), and a poor solvent for PS ($\chi_{PS/DCE}$ = 0.4). Consequently, PS-rich and PLA-rich phases produced by the phase separation process are not equally swollen, which is not in favor of a mediation of the surface energy of the phases in formation. PLA migrates at both interfaces (surface between silicon and polymer and surface of the film) and PS-rich phase is rejected between these two PLA-rich phases. This three-layer morphology (PLA/PS/PLA) is observed for high withdrawal speed (high evaporation rate) when the PS is the major component in the blend (Fig. 2e and f). For lower speed (lower evaporation rate as previous demonstrated), the phase separation proceeds to a higher extent, allowing the three-layer morphology to evolve to more advanced state where PS-rich phase forms discrete domains on a wetting PLA layer (Fig. 2d). The fragmentation of the intermediate PS layer could involve dewetting process as already proposed for the morphology formation in thin films of polymer blends formed by spin-coating [38]. The same fragmentation process is likely to occur when PS is the minor component in the blend (PS:PLA(30:70)) (Fig. 3d–f) where discrete PS domains are formed instead of a three layer morphology (in this latter case a thin residual PLA layer on top of the PS domains is in favor of this mechanism).

4. Conclusion

We demonstrated that the morphology of the dried films, for a given polymer/solvent pair can be driven by the deposition parameters (withdrawal speed and geometry of the reservoir) which allow much more opportunities compared to the spin-coating process where the morphology in the latter case is mostly driven by the composition of the solution to be deposited. We have interpreted the various morphologies obtained (layers and laterally phase-separated domains) by considering the superposition of different phenomena such as phase separation process, dewetting and vitrification. Parameters such as the drying time, the compatibility of the polymer/solvent pairs and the affinity of the polymer towards the interfaces were suspected to play a great role in the control of the morphologies. In this context, the process of dip-coating was carefully examined within the capillary and the draining regimes (for low and high withdrawal speed respectively) in order to get a full description of the thickness variation and evaporation rate as a function of the deposition parameters. This study is of high interest for the control of the morphology in thin films of polymer blends which are considered as serious candidates for advanced functional systems such as sensors, photovoltaic devices or smart templates for lithographic applications.

Conflict of interest

The authors declare no competing financial interest.

Acknowledgments

This project is supported by the region “Centre” through the SUSCRYPP project. We would like to acknowledge the “S2E2 pôle de compétitivité” for its endorsement. Alexandre Noël and Laura

Autrechy are acknowledged for their help to the samples preparation.

Appendix A. Supplementary data

Supplementary data associated with this article can be found, in the online version, at http://dx.doi.org/10.1016/j.apsusc.2016.09.151.

References

[1] S.Y. Heriot, R. Jones, An interfacial instability in a transient wetting layer leads to lateral phase separation in thin spin-cast polymer-blend films, Nat. Mater. 4 (2005) 782–786.
[2] S. Ebbens, R. Hodgkinson, A.J. Parnell, A. Dunbar, S.J. Martin, P.D. Topham, N. Clarke, J.R. Howse, In situ imaging and height reconstruction of phase separation processes in polymer blends during spin coating, ACS Nano 5 (2011) 5124–5131.
[3] S. Walheim, M. Boltau, J. Mlynek, G. Krausch, U. Steiner, Structure formation via polymer demixing in spin-cast films, Macromolecules 30 (1997) 4995–5003.
[4] A. Budkowski, A. Bernasik, P. Cyganik, J. Raczkowska, B. Penc, B. Bergues, K. Kowalski, J. Rysz, J. Janik, Substrate-determined shape of free surface profiles in spin-cast polymer blend films, Macromolecules 36 (2003) 4060–4067.
[5] T. Liu, R. Ozisik, R.W. Siegel, Phase separation and surface morphology of spin-coated films of polyetherimide/polycaprolactone immiscible polymer blends, Thin Solid Films 515 (2007) 2965–2973.
[6] P. Müller-Buschbaum, J.S. Gutmann, M. Stamm, Control of surface morphology by the interplay between phase separation and dewetting, J. Macromol. Sci. Part B Phys. B 38 (1999) 577–592.
[7] H. Ogawa, T. Kanaya, K. Nishida, G. Matsuba, Phase separation and dewetting in polystyrene/poly(vinyl methyl ether) blend thin films in a wide thickness range, Polymer 49 (2008) 254–262.
[8] S. Roy, A. Sharma, Self-organized morphological evolution and dewetting in solvent vapor annealing of spin coated polymer blend nanostructures, J. Colloid Interface Sci. 449 (2015) 215–225.
[9] L. Xue, J. Zhang, Y. Han, Phase separation induced ordered patterns in thin polymer blend films, Prog. Polym. Sci. 37 (2012) 564–594.
[10] S. Zhang, Y. Zhu, T. Shi, H. Zhao, J. You, Y. Li, Selective solvent annealing induced phase separation and dewetting in PMMA/SAN blend ultrathin films, J. Polym. Sci. Part B Polym. Phys. 52 (2014) 1243–1251.
[11] M. Faustini, B. Louis, P.A. Albouy, M. Kuemmel, D. Grosso, Preparation of sol-gel films by dip-coating in extreme conditions, J. Phys. Chem. C 114 (2010) 7637–7645.
[12] S. Roland, C.G. Gamys, J. Grosrenaud, S. Boissé, C. Pellerin, R.E. Prud'homme, C.G. Bazuin, Solvent influence on thickness, composition, and morphology variation with dip-coating rate in supramolecular PS-b-P4VP thin films, Macromolecules 48 (2015) 4823–4834.
[13] L. Huang, Z. Hu, K. Zhang, P. Chen, Y. Zhu, Dip-coating of poly(3,4-ethylenedioxythiophene):poly(styrenesulfonate) anodes for efficient polymer solar cells, Thin Solid Films 578 (2015) 161–166.
[14] C.J. Brinker, Dip coating, in: T. Schneller, R. Waser, M. Kosec, D. Payne (Eds.), Chemical Solution Deposition of Functional Oxide Thin Films, Springer, Vienna, 2013, pp. 233–261.
[15] Z. Hu, J. Zhang, S. Xiong, Y. Zhao, Performance of polymer solar cells fabricated by dip coating process, Sol. Energy Mater. Sol. Cells 99 (2012) 221–225.
[16] A. Sidorenko, I. Tokarev, S. Minko, M. Stamm, Ordered reactive nanomembranes/nanotemplates from thin films of block copolymer supramolecular assembly, J. Am. Chem. Soc. 125 (2003) 12211–12216.
[17] I. Tokarev, R. Krenek, Y. Burkov, D. Schmeisser, A. Sidorenko, S. Minko, M. Stamm, Microphase separation in thin films of poly(styrene-block-4-vinylpyridine) copolymer-2-(4'-hydroxybenzeneazo)benzoic acid assembly, Macromolecules 38 (2005) 507–516.
[18] B. Nandan, M.K. Vyas, M. Böhme, M. Stamm, Composition-dependent morphological transitions and pathways in switching of fine structure in thin films of block copolymer supramolecular assemblies, Macromolecules 43 (2010) 2463–2473.
[19] B.K. Kuila, E.B. Gowd, M. Stamm, Supramolecular assembly of poly(styrene)-b-poly(4-vinylpyridine) and 1-pyrenebutyric acid in thin film and their use for nanofabrication, Macromolecules 43 (2010) 7713–7721.
[20] S. Roland, R.E. Prud'homme, C.G. Bazuin, Morphology, thickness, and composition evolution in supramolecular block copolymer films over a wide range of dip-coating rates, ACS Macro Lett. 1 (2012) 973–976.
[21] S. Roland, D. Gaspard, R.E. Prud'homme, C.G. Bazuin, Morphology evolution in slowly dip-coated supramolecular PS-b-P4VP thin films, Macromolecules 45 (2012) 5463–5476.
[22] A. Vital, M. Vayer, C. Sinturel, T. Tillocher, P. Lefaucheux, R. Dussart, Polymer masks for structured surface and plasma etching, Appl. Surf. Sci. 332 (2015) 237–246.
[23] E. Bauer, E. Maurer, T. Mehaddene, S.V. Roth, P. Müller-Buschbaum, Flow in confined geometry introduced by dewetting of ultrathin polystyrene films, Macromolecules 39 (2006) 5087–5094.
[24] C.J. Brinker, A.J. Hurd, G.C. Frye, P.R. Schunk, C.S. Ashley, Sol-gel thin film formation, J. Ceram. Soc. Japan 99 (1991) 862–877.
[25] R.P. Spiers, C.V. Subbaraman, W.L. Wilkinson, Free coating of a Newtonian liquid onto a vertical surface, Chem. Eng. Sci. 29 (1974) 389–396.
[26] L. Landau, B. Levich, Dragging a liquid by a moving plate, Acta Physicochim. URSS XVII (1942) 141–153.
[27] D. Qu, E. Ramé, S. Garoff, Dip-coated films of volatile liquids, Phys. Fluids 14 (2002) 1154–1165.
[28] M. Le Berre, Y. Chen, D. Baigl, From convective assembly to Landau-Levich deposition of multilayered phospholipid films of controlled thickness, Langmuir 25 (2009) 2554–2557.
[29] J. Huang, R. Fan, S. Connor, P. Yang, One-step patterning of aligned nanowire arrays by programmed dip coating, Angew. Chem. Int. Ed. Engl. 46 (2007) 2414–2417.
[30] M. Ghosh, F. Fan, K.J. Stebe, Spontaneous pattern formation by dip coating of colloidal suspensions on homogeneous surfaces, Langmuir 23 (2007) 2180–2183.
[31] H. Uchiyama, D. Shimaoka, H. Kozuka, Spontaneous pattern formation based on the coffee-ring effect for organic–Inorganic hybrid films prepared by dip-coating: effects of temperature during deposition, Soft Matter 8 (2012) 11318–11322.
[32] A. Diethert, P. Müller-Buschbaum, Probing the near-surface composition profile of pressure sensitive adhesive films with X-ray reflectivity, J. Adhesion 87 (2011) 1167–1190.
[33] M. Maleki, M. Reyssat, F. Restagno, D. Quéré, C. Clanet, Landau–Levich menisci, J. Colloid Interface Sci. 354 (2011) 359–363.
[34] P. Müller-Buschbaum, E. Bauer, E. Maurer, S.V. Roth, R. Gehrke, M. Burghammer, C. Riekel, Large-scale and local-scale structures in polymer-blend films: a grazing-incidence ultra-small-angle X-ray scattering and sub-microbeam grazing-incidence small-angle X-ray scattering investigation, J. Appl. Cryst. 40 (2007) s341–s345.
[35] G. Renaud, R. Lazzari, F. Leroy, Probing surface and interface morphology with grazing incidence small angle X-ray scattering, Surf. Sci. Rep. 64 (2009) 255–380.
[36] P. Müller-Buschbaum, E. Bauer, S. Pfister, S.V. Roth, M. Burghammer, C. Riekel, C. David, U. Thiele, Creation of multi-scale stripe-like patterns in thin polymer blend films, Europhys. Lett. 73 (2006) 35–41.
[37] S.V. Roth, M. Kuhlmann, H. Walter, A. Snigirev, I. Snigireva, B. Lengeler, C.G. Schroer, M. Burghammer, C. Riekel, P. Müller-Buschbaum, Colloidal silver nanoparticle gradient layer prepared by drying between two walls of different wettability, J. Phys.: Condens. Matter. 21 (2009) 264012.
[38] P. Mokarian-Tabari, M. Geoghegan, J.R. Howse, S.Y. Heriot, R.L. Thompson, R.A.L. Jones, Quantitative evaluation of evaporation rate during spin-coating of polymer blend films: control of film structure through defined-atmosphere solvent-casting, Eur. Phys. J. E Soft. Matter 33 (2010) 283–289.